Title

Thermal conductance switching based on the actuation of liquid droplets through the electrowetting on dielectric (EWOD) phenomenon

Authors

Cha, G
Kim, C-J
Ju, YS

Publication Date

2016-04-05

DOI

10.1016/j.applthermaleng.2015.11.098

Peer reviewed

THERMAL CONDUCTANCE SWITCHING BASED ON THE ACTUATION OF LIQUID DROPLETS THROUGH THE ELECTROWETTING ON DIELECTRIC (EWOD) PHENOMENON

*Gilhwan Cha, Chang-Jin ñCJò Kim, and Y. Sungtaek Ju**

Mechanical and Aerospace Engineering Department, UCLA
420 Wetwood Plaza, Los Angeles, California, U.S.A.

*) corresponding author. email) sungtaek.ju@ucla.edu

ABSTRACT

Thermal conductance switches enable active and reconfigurable thermal control and management for a wide variety of applications. We demonstrate a thermal conductance switch based on the actuation of liquid droplets in a co-planar electro-wetting-on-dielectric (EWOD) configuration. By eliminating the need for relative motions of two heat transfer surfaces, the device provides a significant advantage in the mechanical design of adaptive thermal control systems. Proof-of-concept devices are constructed and characterized to confirm the mechanism of droplet detachment and attachment for thermal switching. Numerical simulation is performed to elucidate the experimentally measured thermal performance and identify thermocapillary flows as an important contributor to heat transfer for certain dielectric liquids. The present work provides a proof-of-concept demonstration of novel thermal conductance switches and offers physical insights to help systematically design the switches for practical applications.

Key words: thermal conductance switch; active and reconfigurable thermal control; satellite thermal control; electrowetting; thermocapillary.

1. INTRODUCTION

Ability to modulate the thermal conductance in a reversible manner is important in a wide range of applications. These include bolometers with enhanced dynamic ranges [1], pulsed thermoelectric cooling with increased maximum temperature lifts [2], low-power precision temperature control of chip scale atomic clocks [3], solid-state thermal energy harvesting [4], and thermally reconfigurable networks for satellite thermal management [5,6].

Thermal conductance switches enable adaptive thermal control by switching between high and low heat transfer regimes around a set point. Thermal switches are an optimal solution because of the flexibility they provide. They can be applied to only select thermal paths and variable setting points can be specified for different system components.

Thermal conductance switches based on phase change materials, such as wax and shape memory alloys, have been widely studied [3,7]. Electrostatic devices [8,9] control heat transfer by electrostatically attracting thin radiator films to the opposing surfaces and thereby switching the heat transfer mode from inefficient radiation to efficient conduction. Variable emittance devices, such as micro louvers [10] and electrochromic devices [11], have also been investigated. These latter devices, however, were intended only for space applications where radiation is the dominant heat transfer mechanism.

The vast majority of previous thermal switches relied on making or breaking solid-solid contacts. To achieve a strong contrast in thermal conductance between the on- and off-states, heat conduction across the solid-solid interfaces must be very efficient. Very high contact pressure is necessary to minimize the thermal contact resistance between two solids. This requirement, however, has led to a number of reliability and manufacturing challenges, including fatigue, wear, fracture, debris/particle trapping, and other types of mechanical failures.

Compliant thermal interface materials may potentially mitigate some of the problems encountered in solid-conduction-based thermal switches. A prominent example is a dense array of vertically aligned carbon nanotubes. Adhesion between carbon nanotubes and opposing solid surfaces [12] and the resulting delamination failures, however, made it difficult to use nanotube arrays in reversible thermal switches. Furthermore, large contact pressure is still necessary to achieve small thermal contact resistance due to non-uniformity in nanotube heights.

Liquid-based switching devices are promising as they can circumvent the limitations of previous devices based on direct solid-solid contacts. Past studies demonstrated device concepts that incorporate an array of discrete mercury droplets [13] or dielectric liquids [14–16] between two plates. To turn on the switch, the plates must be mechanically displaced relative to each other to touch and deform the droplets for low-resistance thermal contacts.

This mechanical requirement, which also applies for switches based on solid-solid contacts, significantly limits the design and implementation of past thermal switches.

We propose an alternative type of liquid droplet-based thermal conductance switches illustrated in Fig. 1. In this device concept, the shape of liquid droplets is electrically modulated to make or break physical and thermal contacts with the two heat transfer surfaces. We present the design, fabrication and characterization of proof-of-concept devices to validate their operations. Numerical simulation is also conducted to examine the heat transfer characteristics of the devices. Whereas conduction is the dominant heat transfer mechanism for liquid metal droplets, convection induced by the thermocapillary effect is found to play a significant role for certain dielectric liquids with lower thermal conductivities.

2. CO-PLANAR EWOD DEVICE

We propose an elegantly simple system by introducing liquid droplets between two *stationary* plates and then controlling the droplet shapes to switch between high- and low-thermal conductance states. This approach provides great flexibility in the mechanical design of an overall system. It also helps minimize parasitic heat conduction associated with mechanical supporting structures.

An array of droplets can be controlled individually or simultaneously to attach or detach from the top heat transfer surface. A key aspect of this operation is the so-called electrowetting on dielectric (EWOD) phenomenon [17]. The contact angle of a liquid on a solid surface can be changed by applying or removing an electric field between the liquid and the solid. This change becomes reversible if there is a thin dielectric layer separating the liquid from the solid and hence the name EWOD.

EWOD actuation has been demonstrated for a wide variety of liquids, including aqueous solutions, glycerol, and mercury. A large change in contact angle can be achieved by depositing a low-surface energy material, such as Teflon®, on the control electrode to increase the contact angle at zero bias.

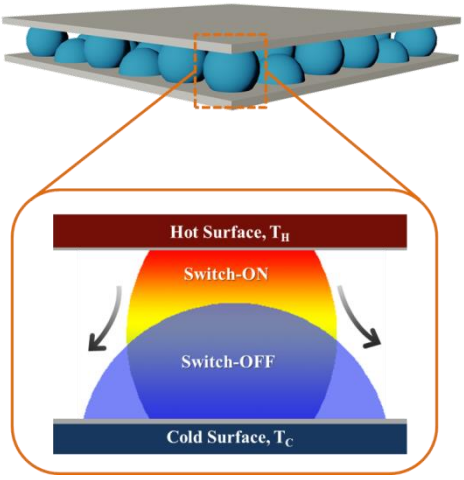

Figure 1: Conceptual design of the proposed co-planar EWOD-based thermal conductance switch.

A switching of droplets between beading and spreading states can also be accomplished using a pair of co-planar electrodes where the ground and bias electrodes are constructed on the same plate [18,19] (Fig. 2). By eliminating the need for placing a second electrode on the opposing plate, the co-planar design greatly simplifies fabrication/assembly processes and provides significant flexibility in optimizing the thermal switch to meet electrical, mechanical as well as thermal requirements.

The operating voltage of a co-planar device with a 500 nm-thick SiO_2 dielectric layer is around 70 V, which can be further reduced through the optimization of electrode geometry and the use of layers with high dielectric constants.

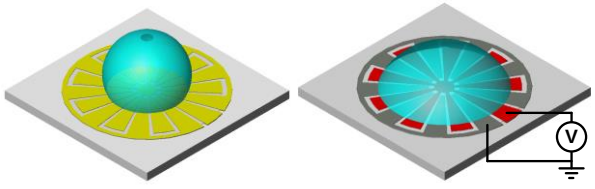

Figure 2: A water sessile droplet switching between the beading and wetting states on the EWOD device with co-planar electrodes [6].

3. DROPLET SWITCHING CRITERIA

Contact angle changes one can achieve using the

EWOD phenomenon are limited by the contact angle saturation phenomenon at high bias voltages, approximately 75° for deionized water. Given such a limit, one needs to determine criteria for successful operations of the thermal conductance switch incorporating a certain liquid.

To successfully operate the thermal switch, the contact angle of a droplet on the bottom surface (θ_{bottom}) and the contact angle change induced by EWOD ($\Delta\theta_{bottom}$) must exceed respective minimum values. For the device to switch on (high thermal conductance state), d_{bottom} must be large enough such that the beading droplet contacts the top surface and form a liquid bridge. For the device to switch off (low thermal conductance state), the contact angle change must be large enough ($\Delta\theta_{bottom} > \Delta\theta_{critical}$) so that the droplet can detach from the top surface. The minimum contact angle change required $\Delta\theta_{critical}$ is a function of the spacing between the two heat transfer surfaces and also of θ_{bottom}. Figure 3 schematically compares the successful and failed droplet detachments for two different values of $\Delta\theta_{bottom}$.

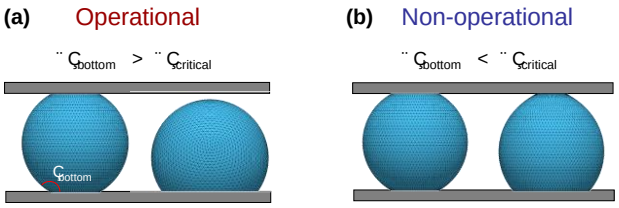

Figure 3: (a) Successful switching operation (Δd_{bottom} = 45° > $\Delta d_{critical}$). (b) Failed operation (Δd_{bottom} < $\Delta d_{critical}$) The liquid droplet shapes are predicted from numerical simulation.

To establish the on-state (or attachment) criterion, we relate the contact angle in the on-state, d_{on}, with the droplet volume V and the spacing between the top and bottom surfaces h. The relationship can be obtained using a geometric analysis for small droplets, which can be approximated as truncated spheres when the gravity effect is negligible (Bond number <<1). The maximum possible spacing, when the droplet just touches the top surfaces, is

$$= \sqrt{\frac{3(1-\cos(\quad))}{(2+\cos(\quad))}}\sqrt[3]{\quad} \qquad (1)$$

The off-state (or detachment) criterion for the contact angle change cannot be established from a simple geometric analysis as we must account for hysteresis in the droplet attachment and detachment processes. Once a liquid forms a liquid bridge, it may form an elongated necked region and remain attached to the top surface even when the two surfaces are moved apart beyond h_{max}. That is, the liquid bridge ruptures only when the spacing between the plates is much greater than h_{max}.

We perform numerical simulations based on the interfacial energy minimization algorithm to determine the rupture distance of liquid bridges as a function of the contact angle on the bottom surface. The equilibrium shape of a liquid bridge is predicted by iteratively finding (or evolving) the bridge shape until we achieve the least total surface energy for a given liquid volume and a given spacing between the top and bottom surfaces. The procedure is repeated for different values of the gap for a given contact angle on the bottom surface. When the gap exceeds a certain critical value, a liquid bridge is no longer a configuration with the least surface energy. This critical value is considered the rupture distance. This then allows us to determine the minimum contact angle change necessary to detach the liquid from the top surface and achieve successful operation of the thermal switch.

Figure 4 illustrates the predicted relationships between the gap h and the bottom contact angle, $d_{bottom,}$ for two different liquids: water and mercury on a substrate coated with Teflon®. The gap has been normalized with respect to the characteristic droplet length scale $V^{1/3}$. For a given initial (zero electric bias voltage) contact angle, one can determine the maximum gap h_{max} one can have while allowing the droplet to contact the top surface and form a bridge. The dashed line shows $h_{max}/V^{1/3}$ for the attachment as a function of the (initial) bottom contact angle. The solid lines show the predicted values of the normalized gap $h/V^{1/3}$ for the detachment as a function of the bottom contact angle in the presence of an operating EWOD bias voltage.

In practical design involving a specific liquid, one can use Fig. 4 to calculate the minimum necessary contact angle change on the bottom surface by first determining the gap necessary to ensure droplet attachment for a given d_{on} (attached or on-state under zero electric bias voltage) and then reading off the value of d_{off} (detached or off-state under an operating EWOD bias voltage) corresponding to this gap. The difference between the two angles, $\Delta\theta_{bottom} = d_{on} - d_{off}$, is the minimum necessary contact angle change. As

a concrete example, we consider using a water droplet on Teflon® surfaces. The contact angle on both the top and bottom surfaces is approximately 120° under zero electrical bias. We read from the plot the minimum required contact angle change $\Delta\theta_{\min,\ water}$ of 39° for successful operation of the switch.

In plotting Fig. 4, we also consider the possibility that the contact angle on the top surface may differ from that on the bottom surface due to temperature-dependence of the surface tension or hysteretic effects. Figure 4 shows three curves for the detachment of water, each corresponding to θ_{top} = 100°, 110°, or 120°, respectively.

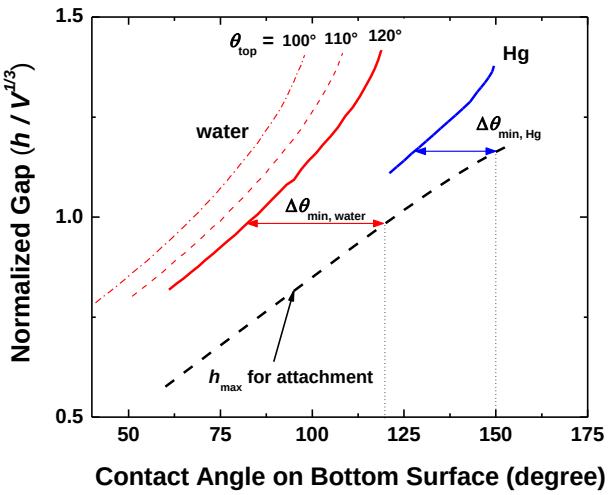

Figure 4: The predicted normalized gap as a function of the contact angle on the bottom surface for liquid bridges of water and mercury. The initial (zero electric field) contact angle of water at the bottom surface is fixed at 120° and that of mercury at 150°.

4. EXPERIMENTAL

The operation and thermal characteristic of our device concept is studied using a single-droplet test vehicle and a microfabricated thin-film heater. Figure 5 shows the process flow to fabricate and assemble our co-planar EWOD thermal switch devices. First, an EWOD device is fabricated on a partially oxidized silicon substrate or a glass substrate. We deposit a 10 nm Cr/100 nm Au layer on the substrate and pattern it to define the co-planar EWOD electrodes. A silicon nitride layer of thickness 500 nm is deposited by plasma-enhanced chemical vapor deposition to serve as an insulation layer for the EWOD electrode arrays. A 200 nm-thick Teflon® layer is spin coated on the silicon nitride layer to turn the surface hydrophobic. Figure 6 shows the top view and cross-sectional view of the finished device on a glass substrate.

To prepare the top substrate with an embedded thin film heater/thermometer, a 100-nm-thick Au film is deposited on a glass plate and lithographically patterned into a serpentine shape, which serves as a planar heater and also an electrical resistance thermometer. The other side of the top plate is uniformly coated with Teflon®. We note in passing that the thermal resistances of the thin films and their interfaces (10^{-8}~10^{-6} m^2 K/W) are several orders magnitude smaller than the overall thermal resistance of our thermal switches incorporating millimeter scale liquid droplets.

The experimental configuration for characterizing the thermal performance of the device is schematically shown in Fig. 7. The switch is placed on a temperature-controlled substrate holder. A liquid droplet is dispensed at the center of the device using a micropipette. The top substrate is transparent (except the heater line) to facilitate visual alignment and is mounted on an extension arm of a precision z-stage to allow the spacing between the top and bottom substrate to be adjusted. A video microscope is used to capture video images of the liquid droplet under EWOD actuation, which are analyzed to extract the geometric parameters of the liquid droplets/bridges.

(a) Deposit a 10nm Cr/100nm Au layer either on a glass slide or on a thermally oxidized silicon wafer and pattern the layer to define the coplanar EWOD electrodes

(b) Deposit a 500nm silicon nitride layer as an electric insulator

(c) Spin-coat a 200nm Teflon® layer for a hydrophobic surface

(d) Dispense liquid droplets and place the plate which the serpentine haters are fabricated on.

Figure 5: Process flow for the microfabrication of the EWOD-driven thermal conductance switching test device.

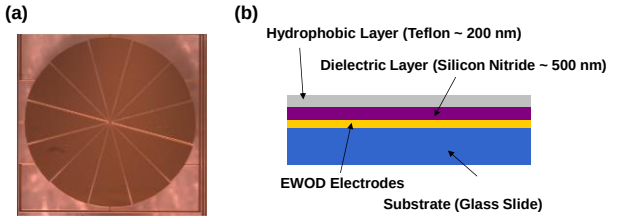

Figure 6: (a) Top view and (b) cross-sectional view of the co-planar EWOD device prepared on a glass substrate. The diameter of the EWOD electrode array is approximately 1.5 mm.

The serpentine heater is subjected to a current pulse and the resulting voltage changes are measured as a function of time. The effective heat flux applied is of the order of $10^3 \sim 10^4$ W/m^2. The time evolution of the temperature changes after pulse initiation is then computed from the pre-calibrated temperature dependence of the electrical resistance of the thin-film heater.

$$R(t) = R_0[1+\alpha\Delta T(t)] \qquad (2)$$

Here, $R(t)$ is the resistance at time t, R_0 is the resistance right before the transient pulse, . is the WHPSHUDWXUH FRHIILFLHQW RI UHVLVWDQFH DQG ΔT is the temperature rise in the heater.

The uncertainty in the measured temperature changes is estimated to be 0.2 °C, dominated by precision errors in the thermometer readings during calibration. The relative error within each temporal temperature profiles is expected to be much smaller. The uncertainty in the dimensions of the substrates and the liquid droplets extracted from optical images is estimated to be approximately 10 μm, limited by the resolution of the imaging system.

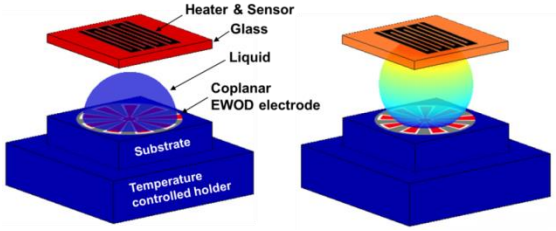

Figure 7: Schematic of the experimental configuration, with the thermal switch in the off (left) and on (right) state. The top surface is heated using an embedded thin-film heater while the bottom substrate is maintained at a constant temperature.

5. RESULTS AND DISCUSSION

Figure 8 shows representative optical images (side views) of a water droplet in the on- and off-state. The droplet shapes predicted using the surface energy minimization algorithm are overlaid on the images, which agree very well with each other. The spacing between the top and bottom substrates is approximately 1 mm.

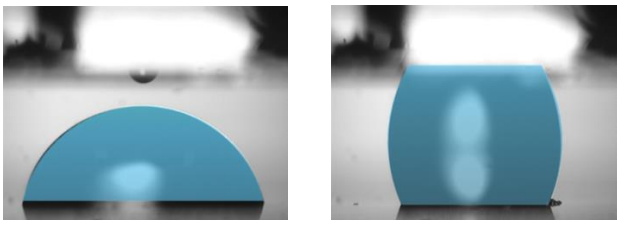

Figure 8: Optical images of a water droplet switching on and off on the coplanar EWOD device driven at a bias voltage of 70 V_{p-p}. The predicted droplet shapes are overlayed on the experimentally obtained images.

We perform numerical simulations of heat transfer using a commercial FEM code. The droplet shapes predicted using the surface energy minimization algorithm are directly imported into the FEM models to enable rigorous heat transfer simulation. The axi-symmetric transient heat diffusion equation is solved for the solids and the gas and the transient energy equation coupled with the Navier-Stokes equations are solved for the liquid to predict the temperature fields and heat transfer rate in the on- and off-state of the thermal switch. The mesh independence study is performed to verify that doubling the number of mesh elements does not change the predicted temperature rises by more than 1 %. The properties of the liquids used in the simulation are summarized in Table 1. The thickness of the glass substrates is 150 μm and the thermal conductivity, measured using the 3ω technique, is 1.2 W/m K.

The heat transfer test results for a water droplet are shown in Fig. 9 together with FEM simulation results. The experimental data for the off-state agree well with the prediction but the data for the on-state deviate substantially from the prediction when it accounts for only pure heat conduction (dotted line). This suggests significant heat transfer augmentation by (an)other mechanisms.

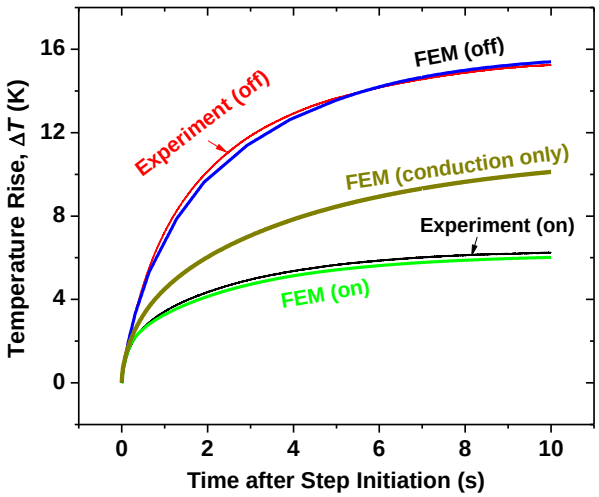

Figure 9: Measured and predicted temporal temperature profiles in the thin-film heater under stepped heating in the on- and off-state of an EWOD-actuated water droplet. The plot shows both FEM prediction considering heat conduction only and FEM prediction considering also thermocapillary flows.

Surface tension is caused by molecular interactions at the interface between two immiscible fluids. For most fluids, surface tension decrease with increasing temperatures. Spatial variations in temperature along the interface lead to corresponding spatial variations in surface tension. These variations result in a tangential stress at the interface, which in turn creates bulk fluid motions inside the droplet and augments heat transfer.

To further investigate the contribution of themocapillary flows to heat transfer in our thermal switch, we consider three different liquids: water, glycerol, and mercury. The parameter that characterizes the strength of thermocapillary flows is the Marangoni number, which is defined as

$$Ma = \frac{\gamma_T d\Delta T}{\rho \nu \alpha} \qquad (3)$$

Here, is the first derivative of the surface tension with respect to the temperature, d is the characteristic length, ΔT is the temperature difference, $\breve{U}$ is the thermal diffusivity, ν is the kinematic viscosity, and $\jmath$ is the liquid density. The Marangoni number of water is greater than that of glycerin by a factor of almost 3000 mainly because water is much less viscous than glycerin (Table 1).

To have a fair comparison, the same geometry is assumed for all three liquids although the actual geometries slightly differ due to difference in their surface tension. On the free surface, the shear stress due to fluid motions is balanced by the stress arising from the temperature gradient along the interface:

$$\mu \frac{\partial v}{\partial x} = \gamma_T \frac{\partial T}{\partial y} \qquad (4)$$

Here v is the tangential velocity. The flow is assumed to be laminar. The Boussinesq approximation is used to account for the buoyancy force.

Figure 10 shows the predicted temperature and velocity fields in the liquid bridges of the three different liquids. The spatial temperature distribution is altered considerably for the water droplet due to a thermocapillary flow when compared with the droplets of glycerin and mercury. These results suggest that one needs to consider not only the thermal conductivity but also the Marangoni number in selecting optimal liquids for a given application.

The experimental data and numerical simulation results in Fig. 9 for a water droplet agree well with each other when both conduction and convection due to thermocapillary flows are taken into account. The observed switching ratio (on-state conduction to off-state conductance) of approximately 2.4 is rather low but it includes the deleterious impact of significant parasitic heat conduction across the air and heat spreading by conduction along the top plate. Switching ratios of the order of 100 are projected for vacuum-packaged thermal switches incorporating arrays of liquid droplets.

Figure 11 shows the experimental data and corresponding numerical predictions for the switch with mercury as the droplet liquid. The experimental data and the simulation results again agree well with each other even when the pure conduction alone is considered. The contribution of the thermocapillary flow is small due in part to the high thermal conductivity of mercury (approximately 7 W/m K at room temperature).

Table 1: Thermophysical properties at 20 °C of the liquids used in the modeling. k: thermal conductivity, γ: surface tension, λ_T: temperature coefficient of surface tensions, μ: dynamic viscosity, ρ: density, C_p: specific heat, Ma: Marangoni number, and β: thermal expansion coefficient.

	k (W/m K)	γ (mN/m)	λ_T (mN/m K)	μ (Pa s)	ρ (kg/m^3)	C_p (J/kg K)	Ma	β (10^{-6}/K)
Water	0.6	72.8	-0.167	8.94×10^{-4}	998	4179	12985	207
Glycerin	0.29	64.0	-0.0598	1.5	1261	2427	4.21	615
Mercury	8.7	483	-0.22	1.53×10^{-3}	13564	139.3	313	182

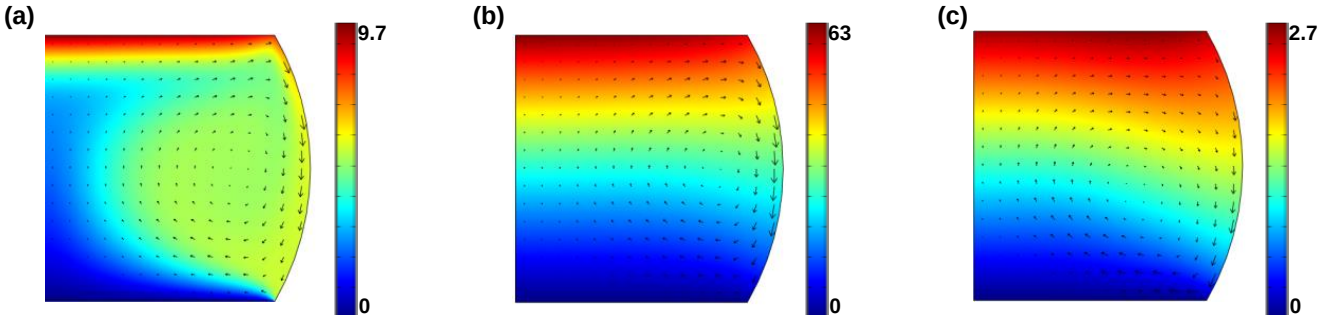

Figure 10: Predicted spatial distributions of the relative temperature rise for the three different liquids (water, glycerol, and mercury). The arrows show the directions of the predicted internal flows in the three liquid droplets.

The observed switching ratio (approximately 2.7) for a mercury droplet with a diameter of approximately 1 mm is comparable to that observed for a water droplet. This is surprising since the thermal conductivity of mercury is an order of magnitude higher than that of water. This is due in part to the smaller droplet-plate contact area of the mercury droplet and in part to the negligible heat transfer enhancement by thermocapillary flows.

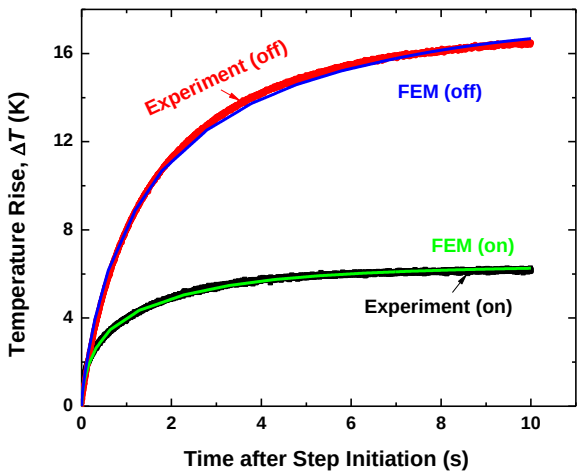

Figure 11: Experimentally measured and predicted temporal temperature profiles experienced by the thin-film heater of the top plate under stepped heating for an EWOD-actuated mercury droplet.

Although the size of a mercury droplet used in the experiment was comparable to the capillary length for mercury (= √ / ≈ 2 mm), the gravity still plays an appreciable role in determining the shape of the mercury droplet. Figure 12 shows the droplet shapes predicted using the surface energy minimization algorithm with or without gravity for water and mercury. The contact area between the mercury droplet and the top plate is significantly reduced under gravity.

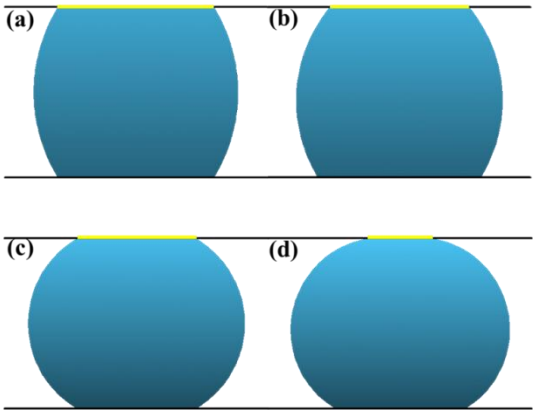

Figure 12: Predicted liquid bridge shapes: (a) water with no gravity (b) water under gravity (c) mercury with no gravity (d) mercury under gravity.

When extrapolated to actual in-space operating conditions, the switch on-off ratio of the order of 1000 can be achieved using low-vapor-pressure liquid metals, such as non-toxic alloys of In-Ga, or low-viscosity ionic liquids with strong thermocapillary potential.

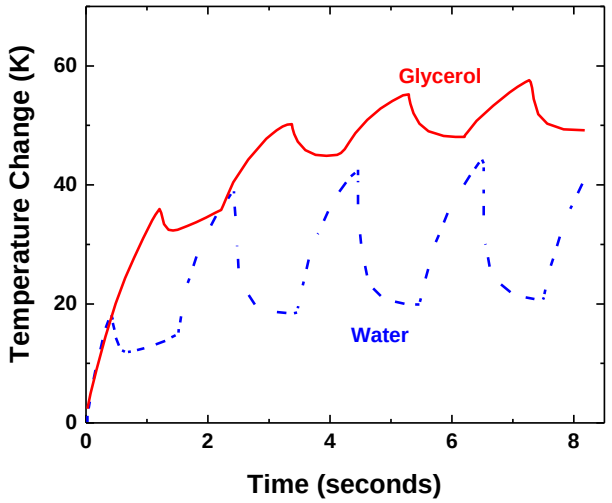

Figure 13: Experimental data from 1 Hz cyclic on-off thermal switching tests using water and glycerol droplets.

A cyclic on-off test is also performed at 1 Hz (Fig. 13) to demonstrate the reversibility of our thermal switches. The response of the thermal switch is much faster with water due in part to the more efficient heat transfer due to thermocapillary flows and to its higher thermal conductivity.

To examine the effect of droplet size in the heat transfer performance, we perform a series of numerical simulations for droplets of different sizes. Figure 14 shows the predicted on-state thermal conductance with and without thermocapillary flows. The on-state thermal conductance increases with decreasing droplet size. As the conduction resistance is reduced with decreasing droplet sizes, however, the relative contribution of convection due to thermocapillary flows also becomes smaller.

The present study used water and mercury as they are well-known heat transfer liquids. The high vapor pressure/evaporation (for water) and health/environmental hazards (for mercury), however, are problematic. For vacuum and space applications, in particular, ionic liquids with nearly zero vapor pressure are promising for the thermal conductance switches proposed here.

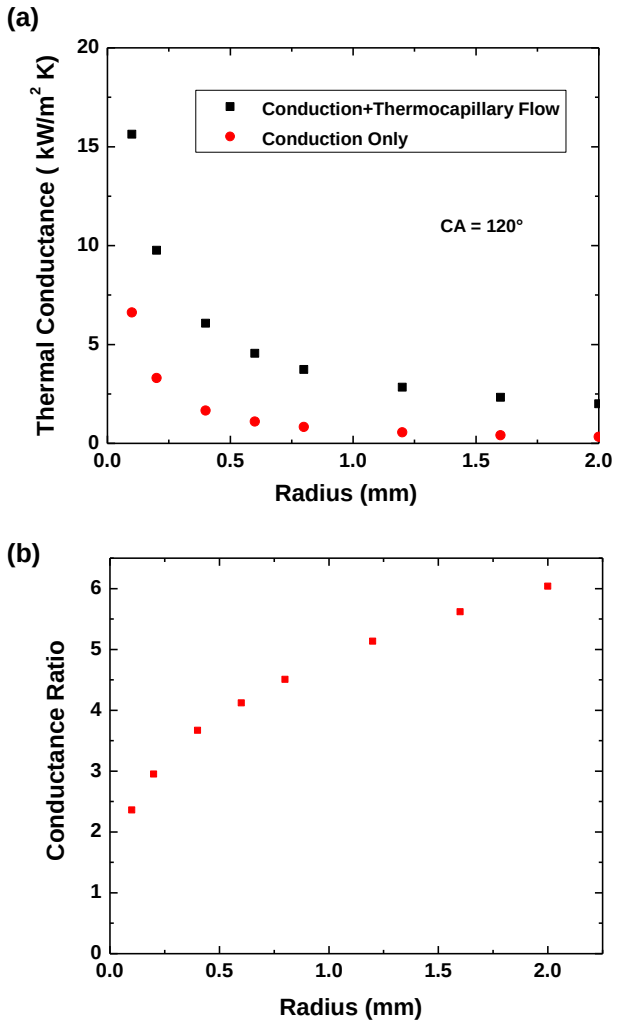

Figure 14: The predicted effect of the droplet size on heat transfer performance for water: (a) on-state thermal conductance for water droplets of different sizes with and without thermocapillary flows (b) ratio of the on-state thermal conductances with and without thermocapillary flows.

6. Summary and Conclusion

We propose and demonstrate a novel liquid-droplet-based thermal switch using coplanar electro-wetting-on-dielectric (EWOD) configuration. We perform numerical simulation based on the surface energy minimization algorithm to determine the switching criteria. By fabricating and testing the proof-of-concept devices, we confirm the mechanism of droplet detachment and attachment through EWOD actuation and has established basic feasibility of novel liquid-droplet-based thermal switches that can overcome limitations of existing solid-conduction-based thermal switches. Analyses of the device characterization results using numerical heat transfer simulation also show that thermocapillary flows in dielectric liquids can significantly enhance heat transfer across liquid bridges made thereof. Dielectric liquids with high Marangoni numbers may therefore offer alternatives to liquid metals.

ACKNOWLEDGEMENTS

This work was based in part on work supported by AFOSR through Grant FA9550-06-01. The authors also acknowledge the technical assistance from Mr. Abolfazl Sadeghpour in revising the figures.

REFERENCES

[1] W.-B. Song, M.S. Sutton, J.J. Talghader, Thermal contact conductance of actuated interfaces, Appl. Phys. Lett. 81 (2002) 1216–1218. doi:doi:10.1063/1.1499518.

[2] U. Ghoshal, Y.S. Ju, A. Miner, M.B. Ketchen, Advanced electronic microcoolers, in: IEEE, 1999: pp. 113–116. doi:10.1109/ICT.1999.843346.

[3] A. Laws, R.Y.J. Chang, V.M. Bright, Y.C. Lee, Thermal Management for Chip-Scale Atomic Clocks, in: American Society of Mechanical Engineers, 2005: pp. 741–745. doi:10.1115/IPACK2005-73444.

[4] G. Cha, Y.S. Ju, Pyroelectric Energy Harvesting using Liquid-Based Switchable Thermal Interfaces, Sens. Actuators Phys. 89 (2013) 100–107.

[5] T.D. Swanson, G.C. Birur, NASA thermal control technologies for robotic spacecraft, Appl. Therm. Eng. 23 (2003) 1055–1065. doi:10.1016/S1359-4311(03)00036-X.

[6] A.D. Williams, S.E. Palo, Modeling and analysis of a robust thermal control system based on forced convection thermal switches, in: International Society for Optics and Photonics, 2006: pp. 622108–622108–11. doi:10.1117/12.665847.

[7] E. Sunada, K. Lankford, M. Pauken, K.S. Novak, G. Birur, Wax-actuated heat switch for Mars surface applications, in: AIP Conf. Proc., AIP Publishing, 2002: pp. 211–213. doi:10.1063/1.1449727.

[8] W. Biter, S. Oh, S. Hess, Electrostatic switched radiator for space based thermal control, AIP Conf. Proc. 608 (2002) 73–80. doi:doi:10.1063/1.1449710.

[9] W. Biter, S. Hess, S. Oh, D. Douglas, T. Swanson, Electrostatic radiator for satellite temperature control, in: 2005 IEEE Aerosp. Conf., 2005: pp. 781–790. doi:10.1109/AERO.2005.1559370.
[10] A. R. Osiander, S.L. Firebaugh, J.L. Champion, D. Farrar, M.A.G. Darrin, Microelectromechanical devices for satellite thermal control, IEEE Sens. J. 4 (2004) 525–531. doi:10.1109/JSEN.2004.830297.
[11] H. Demiryont, K.C.S. Iii, Variable Emittance Electrochromic Devices for Satellite Thermal Control, in: AIP Conf. Proc., AIP Publishing, 2007: pp. 51–58. doi:10.1063/1.2437440.
[12] Y. Zhao, T. Tong, L. Delzeit, A. Kashani, M. Meyyappan, A. Majumdar, Interfacial energy and strength of multiwalled-carbon-nanotube-based dry adhesive, J. Vac. Sci. Technol. B Microelectron. Nanometer Struct. 24 (2006) 331–335. doi:10.1116/1.2163891.
[13] J. Cho, T. Wiser, C. Richards, D. Bahr, R. Richards, Fabrication and characterization of a thermal switch, Sens. Actuators Phys. 133 (2007) 55–63. doi:10.1016/j.sna.2006.03.033.
[14] G. Cha, Y.S. Ju, Reversible thermal interfaces based on microscale dielectric liquid layers, Appl. Phys. Lett. 94 (2009) 211904. doi:10.1063/1.3142866.
[15] Y. Jia, G. Cha, Y.S. Ju, Switchable Thermal Interfaces Based on Discrete Liquid Droplets, Micromachines. 3 (2012) 10–20. doi:10.3390/mi3010010.
[16] Y. Jia, Y.S. Ju, Solid-Liquid Hybrid Thermal Interfaces for Low-Contact Pressure Thermal Switching, J. Heat Transf. 136 (2014) 074503–074503. doi:10.1115/1.4027205.
[17] W.C. Nelson, C.-J. "CJ" Kim, Droplet Actuation by Electrowetting-on-Dielectric (EWOD): A Review, J. Adhes. Sci. Technol. 26 (2012) 1747–1771. doi:10.1163/156856111X599562.
[18] U.-C. Yi, C.-J. Kim, Characterization of electrowetting actuation on addressable single-side coplanar electrodes, J. Micromechanics Microengineering. 16 (2006) 2053–2059. doi:10.1088/0960-1317/16/10/018.
[19] J. Gong, G. Cha, Y.S. Ju, C.-J. Kim, Thermal switches based on coplanar EWOD for satellite thermal control, in: IEEE 21st Int. Conf. Micro Electro Mech. Syst. 2008 MEMS 2008, 2008: pp. 848–851. doi:10.1109/MEMSYS.2008.4443789.